



Transport of mesospheric H₂O during and after the stratospheric sudden warming of January 2010: observation and simulation

C. Straub¹, B. Tschanz¹, K. Hocke^{1,2}, N. Kämpfer^{1,2}, and A. K. Smith³

¹Institute of Applied Physics, University of Bern, Switzerland

²Oeschger Center for Climate Change Research, University of Bern, Switzerland

³Atmospheric Chemistry Division, National Center for Atmospheric Research, Boulder CO, USA

Correspondence to: C. Straub (corinne.straub@iap.unibe.ch)

Received: 20 October 2011 – Published in Atmos. Chem. Phys. Discuss.: 12 December 2011

Revised: 12 May 2012 – Accepted: 4 June 2012 – Published: 22 June 2012

Abstract. The transportable ground based microwave radiometer MIAWARA-C monitored the upper stratospheric and lower mesospheric (USLM) water vapor distribution over Sodankylä, Finland (67.4° N, 26.6° E) from January to June 2010. At the end of January, approximately 2 weeks after MIAWARA-C's start of operation in Finland, a stratospheric sudden warming (SSW) disturbed the circulation of the middle atmosphere. Shortly after the onset of the SSW water vapor rapidly increased at pressures between 1 and 0.01 hPa. Backward trajectory calculations show that this strong increase is due to the breakdown of the polar vortex and meridional advection of subtropical air to the Arctic USLM region. In addition, mesospheric upwelling in the course of the SSW led to an increase in observed water vapor between 0.1 and 0.03 hPa.

After the SSW MIAWARA-C observed a decrease in mesospheric water vapor volume mixing ratio (VMR) due to the subsidence of H₂O poor air masses in the polar region. Backward trajectory analysis and the zonal mean water vapor distribution from the Microwave Limb Sounder on the Aura satellite (Aura/MLS) indicate the occurrence of two regimes of circulation from 50° N to the North Pole: (1) regime of enhanced meridional mixing throughout February and (2) regime of an eastward circulation in the USLM region reestablished between early March and the equinox. The polar descent rate determined from MIAWARA-C's 5.2 parts per million volume (ppmv) isopleth is $350 \pm 40 \text{ m d}^{-1}$ in the pressure range 0.6 to 0.06 hPa between early February and early March. For the same time interval the descent rate in the same pressure range was determined using Transformed Eulerian Mean (TEM) wind fields simulated by

means of the Whole Atmosphere Community Climate Model with Specified Dynamics (SD-WACCM). The average value of the SD-WACCM TEM vertical wind is 325 m d^{-1} while the along trajectory vertical displacement is 335 m d^{-1} . The similar descent rates found indicate good agreement between the model and MIAWARA-C's measurements.

1 Introduction

Water vapor enters the stratosphere from the equatorial troposphere through the tropical tropopause layer from where it is transported upward into the mesosphere following the Brewer-Dobson circulation (Andrews et al., 1987). As the tropical tropopause layer acts as a cold trap the whole middle atmosphere is extremely dry (Brewer, 1949). The positive vertical gradient throughout the stratosphere is due to the second source of H₂O in the middle atmosphere, the oxidation of methane while the negative vertical gradient in the mesosphere is mainly caused by photo-dissociation due to the absorption of solar Lyman α radiation (Brasseur and Solomon, 2005).

The chemical lifetime of water vapor is in the order of months in the lower mesosphere and in the order of weeks in the upper mesosphere (Brasseur and Solomon, 2005). This is long with respect to dynamical processes and water vapor is therefore a tracer for atmospheric transport. The zonal mean distribution of water vapor in December 2009 as measured by Aura/MLS (Waters et al., 2006) is displayed in Fig. 1. As the vertical H₂O gradient is negative throughout the mesosphere, dry air from the upper mesosphere can be used to

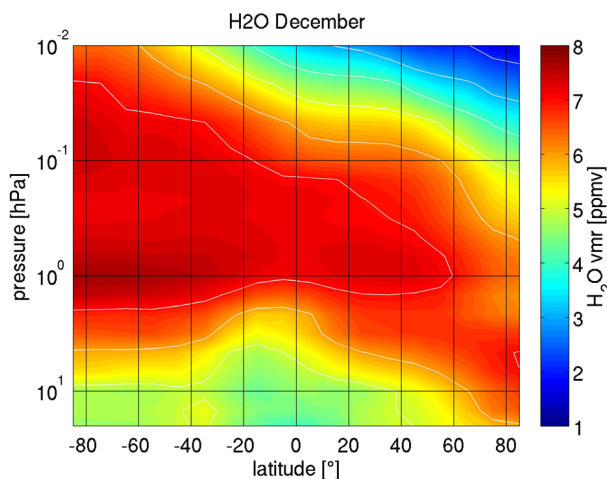


Fig. 1. Zonal mean distribution of middle atmospheric water vapor as measured by EOS/MLS through December 2009. Red indicates relatively higher values and blue relatively lower values.

investigate polar winter descent and humid air from around the stratopause for polar summer ascent. The polar winter descent induces horizontal gradients in the H₂O volume mixing ratio (VMR) as the mesospheric air descending within the polar region is much drier than the air outside of it. Due to this horizontal gradient water vapor is a valuable tracer for short term mixing in the winter hemisphere, e.g. in the course of stratospheric sudden warmings. Around the stratopause H₂O is not a good tracer due to its local maximum in the upper stratosphere (Lee et al., 2011).

Stratospheric sudden warmings (SSW) are extreme events in the middle atmosphere characterized by a fast and strong increase of stratospheric temperature (usually at least 25 K in a week or less) and simultaneous cooling of the mesosphere. The main cause for SSWs are planetary waves excited in the troposphere propagating up into the stratosphere where they interact with the mean flow (Matsuno, 1971; Liu and Roble, 2002). Dissipation of planetary waves decelerates the polar night jet and induces a poleward residual circulation, which produces adiabatic heating due to downward flow in the high latitude stratosphere and adiabatic cooling due to upward flow in the high latitude mesosphere. The forcing by planetary waves can be strong enough to reverse the polar night jet.

In the course of SSWs the stratospheric polar vortex is strongly distorted and either shifted off the pole (vortex displacement event) or even split in two pieces (vortex split event), (Charlton and Polvani, 2006). There has been a strong vortex displacement event in 2006 and a strong vortex split event in 2009. Both SSWs were used to thoroughly study dynamics and transport processes during SSWs (e.g. Coy et al., 2009; Harada et al., 2010; Siskind et al., 2010; Funke et al., 2010). The weakening of the high-latitude transport barrier in the course of a SSW can lead to strong mixing of air masses.

Manney et al. (2008, 2009a,b) investigated transport of the trace gases CO, H₂O and N₂O during the warmings in 2006 and in 2009 using satellite data from Aura/MLS, ACE/FTS and TIMED/SABER and model outputs from SLIMCAT, GEOS5 and ECMWF. These trace gases showed values characteristic of low and mid-latitudes extending to Polar Regions and extremely weak gradients throughout the hemisphere. Approximately 3 weeks after both the 2006 and 2009 SSWs, the vortex in the upper stratosphere and lower mesosphere (USLM) reformed, reestablishing the mixing barriers and strong diabatic descent developed, echoing the pattern of descent typically seen in fall, see e.g. Siskind et al. (2007), Orsolini et al. (2010), Smith et al. (2011) and references therein.

The fall and winter descent in the USLM vortex can be regarded as a part of the mesospheric branch of the Brewer-Dobson circulation (Brewer, 1949). The determination of the velocity of polar winter descent is of scientific interest as it provides important information for the characterization of the meridional circulation.

Fall descent rates for the upper stratosphere in both hemispheres have been modeled by Manney et al. (1994) who obtained a value of approximately 260 m d⁻¹ for the 1992/1993 Arctic vortex. In addition there have been studies investigating the descent rate in the Arctic/Antarctic middle atmosphere using ground based measurements. Forkman et al. (2005) determined fall descent rates of up to 300 m d⁻¹ at 75 km altitude at 60° N using CO and H₂O data while Allen et al. (2000) found Antarctic fall descent rates of 250 m d⁻¹ at 60° S and 330 m d⁻¹ at 80° S in the upper stratosphere using CO data.

There have only been few studies investigating USLM descent rates after SSWs. Using observations of Aura/MLS and Empirical Orthogonal Function analysis Lee et al. (2011) determined descent rates of approximately 1500 m d⁻¹ at 80 km decreasing linearly to 500 m d⁻¹ at 60 km for the time after the 2006 and 2009 SSWs. Salmi et al. (2011) found mesosphere to stratosphere descent rates of approximately 700 m d⁻¹ after the 2009 SSW using NO_x data from ACE/FTS and the FinROSE chemical transport model. After the SSW of February 2004 Nassar et al. (2005) estimated a descent rate of 150 m d⁻¹ in the upper stratosphere from CH₄ and H₂O measurements of ACE/FTS.

There have been previous studies using data of ground based microwave radiometers to investigate the stratospheric and mesospheric response to SSWs. Seele and Hartogh (2000) demonstrated that ground based measurements of mesospheric water vapor can be used to monitor transport processes during dynamical events such as SSWs. During a SSW in February 1998 a northward flow transported moist air from lower latitudes to northern Scandinavia resulting in an increase in mesospheric water vapor. Flury et al. (2009) investigated ozone depletion and water vapor enhancement at mid-latitudes during the SSW 2008 using trajectory calculations. They showed that the water vapor enhancement

was associated with meridional transport while the observed ozone depletion was mainly due to temperature-dependent photochemistry in the upper stratosphere (above 5 hPa) and mainly due to transport of polar air to mid-latitudes in the lower stratosphere (below 5 hPa). de Wachter et al. (2011) observed a decrease in mesospheric water vapor over Seoul, South Korea, during the SSW 2008 which they attributed to polar air being transported to such low latitudes when the polar vortex was shifted towards Europe in the course of the SSW.

In this paper we investigate horizontal transport throughout the mesosphere during and after the SSW 2010 using backward trajectory calculations at several mesospheric altitudes. In addition we present post SSW Arctic mesospheric descent rates determined from ground based and space borne water vapor measurements and TEM vertical wind and trajectory calculations. To our knowledge this is the first study investigating polar descent after a SSW using ground based data.

The article is organized as follows. Sections 2 and 3 present the measured and modeled data sets used. Section 4 introduces the trajectory computations. Section 5 gives an overview about dynamical changes during the SSW of January 2010. Section 6 presents the measured water vapor distribution and discusses influences of the SSW upon it. Section 7 shows conclusions drawn from this study.

2 Measurement data

Water vapor data from two sources, a ground based and a space borne microwave radiometer, are used in this study.

2.1 Ground based microwave radiometer MIAWARA-C

The first source is measurements of the vertical distribution of H₂O VMR over Sodankylä, Finland (67.4° N, 26.6° E) recorded by the ground based MIddle Atmospheric WAtmospheric vapor RAdiometer MIAWARA-C belonging to the University of Bern, Switzerland. The instrument has been operated at the Finnish Meteorological Institute Arctic Research Center from mid-January to mid-June in the frame of the Lapland Atmosphere-Biosphere Facility (LAPBIAT2) campaign. MIAWARA-C has been specifically designed for measurement campaigns. The instrument has two main functions; it serves as a traveling standard for inter-comparison (Straub et al., 2011; Leblanc et al., 2011; Stiller et al., 2012) and it is used in measurement campaigns focusing on dynamic processes. The instrument is of a compact design and has a simple set up procedure. It can be operated as a standalone instrument as it maintains its own weather station and a calibration scheme that does not rely on other instruments nor the use of liquid nitrogen. Water vapor profiles are retrieved from measured spectra of the pressure broadened 22 GHz

rotational emission line (see Straub et al., 2010, 2011 for details on MIAWARA-C). Here, data from 10 January to 31 March 2010 is considered and analyzed to yield daily estimates of water vapor profiles in an altitude range between 10 and 0.02 hPa (approximately 30 to 75 km) with a vertical resolution of approximately 12 km. The uncertainty on MIAWARA-C's profiles is typical for ground based 22-GHz water vapor radiometers as shown in Straub et al. (2010, 2011). The simulated accuracy (determined as the 2- σ systematic error arising from uncertainties in a priori temperature, in calibration and in spectroscopy) is below 16 % at all altitudes, while the simulated precision (determined by propagation of 1- σ measurement noise) degrades from 5 % at altitudes up to 50 km to 18 % between 50 and 75 km.

2.2 Aura/MLS

The second source of data is the Microwave Limb Sounder (MLS) aboard the Aura satellite described in Waters et al. (2006). Daily zonal averages of H₂O VMR and temperature MLS acquired in the northern hemisphere over the time interval 10 January to 31 March 2010 are considered here. The highest latitude accessible to the satellite is 82.5° N. MLS yields water vapor as one of its version 2.2 level 2 data products covering the pressure range of 316 to 0.002 hPa. The vertical resolution of this retrieval version is 3–4 km in the stratosphere but degrades to approximately 12 km at 0.1 hPa and above. The single profile precision (1- σ random error estimated from the level 2 algorithms) is 4–9 % in the stratosphere and degrades from 6 to 34 % between 0.1 and 0.01 hPa. The accuracy (likely magnitude of 2- σ systematic error) is estimated to be 4 to 11 % for the pressure range 68 to 0.01 hPa (Lambert et al., 2007). The Aura satellite is in a Sun-synchronous orbit passing through two local times at any given latitude. For this analysis zonal mean water vapor at 67° N is used in order to complement MIAWARA-C's point measurements with zonal mean profiles. When using mean values of a number of profiles n it is assumed that the systematic bias (accuracy) is the same as for a single profile while the 1- σ random uncertainty decreases by a factor $1/\sqrt{n}$.

3 Model data

3.1 ECMWF

Meteorological operational reanalysis data (geopotential height, horizontal and vertical wind) from the European Center of Medium-range Weather Forecast (ECMWF) are used for the description of the 2010 SSW in Figs. 2 and 3 and for the Lagrangian trajectory calculations. The documentation of the cycle 36r1 data used in this study can be found in ECMWF (2012a). This data set has 91 vertical levels with 9 mesospheric levels (above 1 hPa) and the upper limit at 0.01 hPa. The grid spacing is 1.125° in latitude and 4.5°

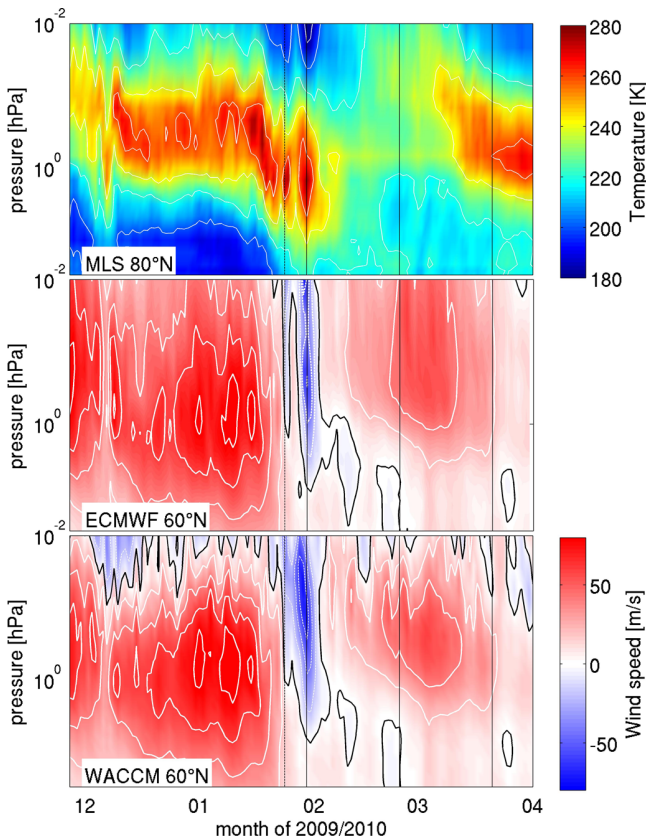


Fig. 2. MLS zonal mean temperature at 80° N and ECMWF and SD-WACCM zonal mean zonal wind at 60° N. Top panel: red relatively higher values and blue relatively lower values. Middle panel: red eastward winds and blue westward winds from ECMWF. Bottom panel: red eastward winds and blue westward winds from SD-WACCM. The vertical lines indicate the following dates (from the left): 24 January (wind reversal mesosphere), 30 January (maximum temperature at 60° N and 10 hPa), 24 February (end of the time of enhanced meridional mixing) and 21 March (equinox).

in longitude. On 26 January 2010 ECMWF's operational data set was updated from version T799 to T1279 (ECMWF, 2012b), i.e. the horizontal resolution has been increased from 25 to 16 km. However, before any new operational implementation, the old and new versions are run side by side. In order to avoid discontinuity in the analyzed data T1279 is used during the whole time.

The mesospheric levels of ECMWF are relatively close to the model top. However, the model still maintains a good representation of gravity wave drag processes and it produces a relatively realistic Brewer-Dobson circulation as shown by Monge-Sanz et al. (2007).

3.2 SD-WACCM

This study presents results from the NCAR Whole Atmosphere Community Climate Model with Specified Dynamics (SD-WACCM). WACCM uses a free-running dynamical core that is adopted from the NCAR Community Atmosphere Model (CAM) and a chemistry module that is an extension of version 3 of the Model of OZone And Related Tracers (MOZART3), e.g. Kinnison et al. (2007). In a recent validation effort, WACCM was shown to perform very well in comparisons with many other chemistry-climate models (SPARC, 2010). For the specified dynamics (SD) runs described in Lamarque et al. (2012), wind and temperature fields are nudged, at each model time step, using the Goddard Earth Observing System 5 (GEOS-5) analysis. The use of the specified dynamics option of WACCM facilitates the comparisons with observations of trace chemical species.

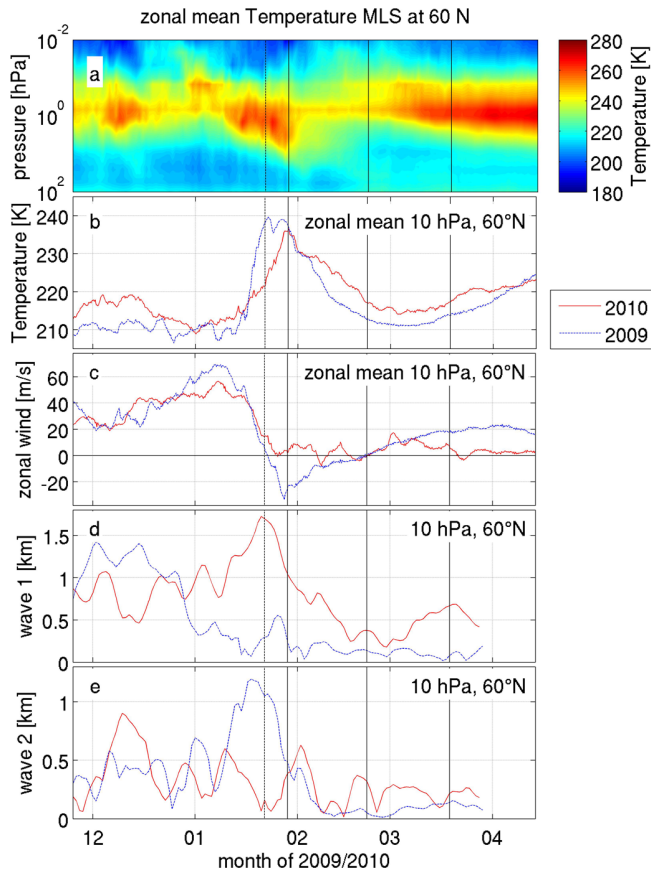


Fig. 3. This figure follows loosely the style of Fig. 1 in Manney et al. (2009b). (a) MLS zonal mean temperature as function of time and pressure at 60° N in 2010 (red relatively higher values, blue relatively lower values), (b) MLS temperature, (c) ECMWF zonal wind, (d) altitude wave 1 from ECMWF and (e) altitude wave 2 from ECMWF. The red curves indicate temperature, zonal mean zonal wind, wave 1 and wave 2 for 2010 while the blue curve indicates corresponding values for the 2009 SSW which occurred at the almost same time of the year (major SSW criterion was fulfilled on 24 January). For details see text. The vertical lines indicate the following dates (from the left): 24 January (wind reversal mesosphere), 30 January (maximum temperature at 60° N and 10 hPa), 24 February (end of the time of enhanced meridional mixing) and 21 March (equinox).

This study presents results from the NCAR Whole Atmosphere Community Climate Model with Specified Dynamics (SD-WACCM). WACCM uses a free-running dynamical core that is adopted from the NCAR Community Atmosphere Model (CAM) and a chemistry module that is an extension of version 3 of the Model of OZone And Related Tracers (MOZART3), e.g. Kinnison et al. (2007). In a recent validation effort, WACCM was shown to perform very well in comparisons with many other chemistry-climate models (SPARC, 2010). For the specified dynamics (SD) runs described in Lamarque et al. (2012), wind and temperature fields are nudged, at each model time step, using the Goddard Earth Observing System 5 (GEOS-5) analysis. The use of the specified dynamics option of WACCM facilitates the comparisons with observations of trace chemical species.

The gravity wave parameterization in WACCM (Richter et al., 2010) determines the mean flow forcing from a discrete spectrum of gravity waves that are forced interactively in the troposphere by topography, convection (mostly in low latitudes), and frontal dynamics (middle and high latitudes). The parameterization also gives a coefficient for vertical eddy diffusion that affects heat and the mixing ratios of trace species.

In the current study, SD-WACCM is nudged with 1 % of the GEOS-5 meteorological fields (e.g. temperature, zonal and meridional winds, and surface pressure) every 30 min. The nudging alters the model predictions by effectively combining $0.99 \times$ the model predicted field with $0.01 \times$ the value from the assimilation model, i.e., $T = 0.99 \times T(\text{WACCM}) + 0.01 \times T(\text{GEOS-5})$. It is applied below 50 km and tapers to zero between 50 and 60 km. The GEOS-5 analysis is available with a time resolution of 6 h and is interpolated to the 30-min nudging intervals. Latitude and longitude resolution for these WACCM runs is $1.9 \times 2.5^\circ$ and there are 88 pressure levels from the surface to 150 km altitude. The nudging allows SD-WACCM to perform as a chemical transport model in the troposphere and stratosphere. The model generates mesospheric dynamical fields, in effect performing as a free-running model above 60 km except that the forcing from below is based on observations.

3.3 Mesospheric wind in the two models

Lower mesospheric winds are poorly observed and therefore models with assimilated data are probably our best way of determining 4 dimensional wind fields at these altitudes. The two models used in this study, ECMWF and SD-WACCM, assimilate data or are nudged with assimilated data, respectively, in the lower and middle stratosphere and are unconstrained in the upper levels. Therefore, the inaccuracy of their wind fields increases with altitude in the mesosphere. However, Liu et al. (2008) show that in WACCM error growth is limited when the lower atmosphere is continually reinitialized, as it effectively is in the SD-WACCM. In addition WACCM includes a physically based gravity wave source parameterization which realistically simulates zonal mean winds (Richter et al., 2010). Still, the mesospheric winds of ECMWF and SD-WACCM suffer under large uncertainties and need to be handled with care. A comparison between the zonal mean zonal winds from the two models is given in the middle and lower panels of Fig. 2 (the discussion of this figure, which in addition shows MLS zonal mean temperature in the top panel, follows in Sect. 5). The plots illustrate that below 0.1 hPa there is a good qualitative agreement between the two data sets while there are major differences even in the wind directions above that level. At altitudes above 0.1 hPa the zonal mean winds of SD-WACCM are regarded as more reliable than those of ECMWF since the upper model boundary of WACCM (approximately 150 km) is higher than the one of ECMWF (approximately 80 km). Therefore, WACCM outputs are used to illustrate zonal mean winds at these alti-

tudes. ECMWF data and Lagrangian backward trajectories are only presented up to 0.1 hPa.

4 Data analysis

This paper presents two different trajectory computation methods with two different information contents: (1) Lagrangian backward trajectories started over Sodankylä giving information on horizontal (zonal and meridional) and vertical origin of air parcels sampled by MIAWARA-C and (2) zonal mean trajectories started at 67°N following the transformed Eulerian mean (TEM) circulation giving information on large scale meridional and vertical advection of air masses due to the combined effects of zonally averaged winds and wave momentum transport.

In general the TEM trajectories are regarded as more reliable than the Lagrangian trajectories especially in the mesosphere. The reason is that zonal mean winds are used for the calculation of the TEM trajectories while for the calculation of the Lagrangian trajectories 4 dimensional wind fields are needed. Nezlin et al. (2009) point out that scales smaller than total horizontal wavenumber 10 are not well represented in the mesosphere by any data assimilation system. As the Lagrangian trajectories are calculated on scales much smaller than wavenumber 10 this introduces a large uncertainty.

However, the authors understand that additional information about mixing processes can be gained from the Lagrangian trajectories despite their large uncertainties.

4.1 Lagrangian backward trajectories

The Lagrangian backward trajectories are computed using the LAGRangian ANalysis TOOl LAGRANTO described in Wernli and Davies (1997) together with the wind fields provided by ECMWF operational data (ECMWF, 2012a).

Daily 3-day backward trajectories are calculated for every USLM pressure level of MIAWARA-C's retrieval grid below 0.1 hPa. As the photo-chemical lifetime of H₂O is in the order of months in the lower mesosphere and weeks in the upper mesosphere, its VMR is assumed to be conserved along the trajectory. The trajectories give the geographical origin of the air masses measured by MIAWARA-C.

As there is no observational information on upper stratospheric and mesospheric water vapor in the ECMWF system the water vapor values along the trajectories are determined from MLS observations. For each trajectory point (each altitude and day) the MLS profiles within $\pm 1^\circ$ in latitude, $\pm 10^\circ$ in longitude and $\pm 0.5\text{ d}$ in time are searched. This search results in one or two profiles per trajectory point. The H₂O VMR values at the altitude closest to the trajectory point are then averaged (if there is more than one profile) and used for the analysis.

4.2 TEM backward trajectories

The TEM circulation describes the bulk motion of large scale air masses as it closely approximates the net air parcel displacement in the latitude-pressure plane (Andrews and McIntyre, 1976). The TEM trajectories are calculated using daily TEM velocities determined from daily averaged WACCM model output. The approach used for the trajectory computations is the same as in Smith et al. (2011). For the analysis presented in this paper the daily backward trajectories are started at 67° N for every USLM pressure level of MIAWARA-C's retrieval grid. For the illustration of short term vertical motion 3-day backward trajectory calculations are shown and 20-day backward TEM trajectories are presented in order to illustrate the residual meridional circulation (Brewer-Dobson circulation).

5 The SSW 2010

5.1 Dynamical overview

The temperature and wind evolution of the 2010 SSW was similar to the major SSW of late January 2009 described in Manney et al. (2009b). The polar stratopause dropped and broke down (nearly isothermal middle atmosphere) and then reformed at a high altitude (~ 0.03 hPa). As this effect is most pronounced at latitudes north of 70° N the temperature evolution at 80° N is displayed in the upper panel of Fig. 2. The lower panel shows the temporal evolution of ECMWF zonal mean zonal wind at the approximate latitude of the polar night jet (60° N). In December and January the polar night jet is visible as an eastward circulation centered around 60° N and 1 hPa. By the end of January the wind rapidly decelerates, the polar vortex shifts towards Europe and the zonal mean temperature at 10 hPa and 60° N increases by approximately 25 K with the maximum on 30 January (second vertical line in the figures). The zonal mean latitudinal temperature gradient is positive in that time. The zonal mean wind reverses at altitudes above 10 hPa and latitudes north of 60° N on 24 January (first vertical line in the figures) with maximum westward wind speeds of 60 m s^{-1} at 0.3 hPa and 65° N on 29 January. After the 2010 SSW the zonal wind in the stratosphere stays weak and the polar vortex does not recover at its original latitude before the circulation reverses to summer easterlies in the end of March (Fig. 2). In the mesosphere an eastward circulation returns approximately 10 days after the wind reversal and by the end of February a USLM vortex forms reestablishing a weak mixing barrier. This is similar to the evolution observed after the SSW 2009 (Manney et al., 2009b) except that in 2010 the post SSW USLM vortex remained weaker than in 2009.

In order to point out similarities and differences a direct comparison between the SSW of January 2010 (red line) and the SSW of January 2009 (blue line) is given in pan-

els b, c, d and e of Fig. 3. As the two warmings occurred at a similar time of the year (in 2009 the major SSW criterion was fulfilled on 24 January) the same axis showing month of 2008/2009 or 2009/2010, respectively is used for both lines. This figure is loosely based on Fig. 1 in Manney et al. (2009b) comparing the SSWs of 2006 and 2009. In January 2009 the anomalous increase in stratospheric temperature was faster and slightly stronger than in 2010. The same is true for the deceleration of the zonal mean zonal wind at 60° N and 10 hPa. In 2009 the zonal wind reversal was accompanied by strong geopotential height wave 2 amplification (vortex split event) while geopotential height wave 1 was strong in December but weakened in the beginning of January. A few days after the maximum temperature slight wave 1 amplification was evident. In the beginning of winter 2009/2010 geopotential height wave 1 was weaker than at the same time of the previous year but it amplified before the SSW in January at the same time as the zonal mean zonal wind decelerated. This indicates that the January 2010 SSW was a vortex displacement event. The amplitude of wave 2 had a peak in mid-December when a minor SSW occurred but stayed fairly weak for the rest of the winter.

5.2 Zonal mean water vapor distribution indicating horizontal mixing and vertical motion

An overview of the northern hemisphere water vapor zonal mean distribution as observed by MLS before, during and after the SSW 2010 is shown in Fig. 4 together with WACCM zonal mean zonal wind. On 15 January, before the SSW, the mixing barrier given by the polar night jet is clearly visible in the form of a maximum in eastward wind at 60° N and 1 hPa and a strong horizontal gradient in mesospheric water vapor VMR with dry air north of 60° N and humid air south of it (panel a). During the SSW, on 30 January, the day of the maximum warming/cooling in the stratosphere/mesosphere, the situation has reversed: now the middle atmospheric zonal wind in the Arctic has changed to westward and the mesosphere (at altitudes above 0.1 hPa) is more humid north of 60° N than south of it (panel b). This situation is short lived and only persists for 3 days. It is linked with the strong mesospheric upwelling in the course of the SSW leading to the observed cooling above 0.1 hPa.

For approximately three weeks after the warming the mean horizontal water vapor distribution in the mesosphere at latitudes between 45 and 82.5° N is close to uniform and the maximum in zonal mean eastward wind is situated at approximately 40° N in the mesosphere (panel c shows 19 February as an example). The disappearance of meridional H₂O gradients indicates strong horizontal mixing between mid-latitudes and the Arctic. Approximately four weeks after the SSW the horizontal H₂O gradient at around 60° N has reappeared indicating that the mixing barrier has reformed (panel d shows 10 March). However, the zonal mean zonal eastward wind does not show any distinct maxima indicating

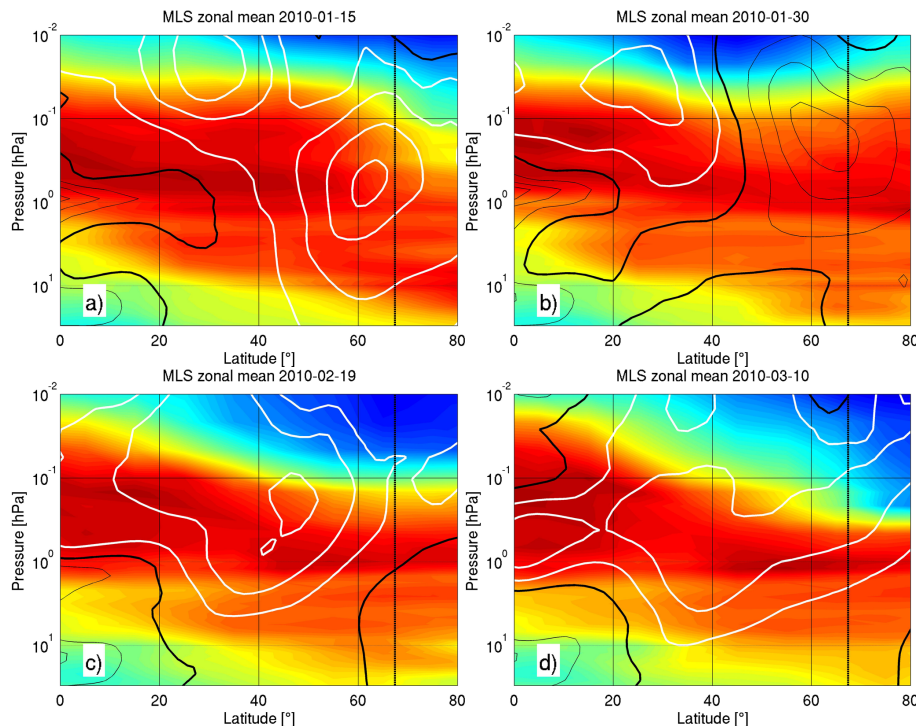


Fig. 4. Evolution of MLS zonal mean H₂O VMR (colors, red relatively higher values, blue relatively lower values) and WACCM zonal mean zonal wind (contours, contour interval = 20 m s^{-1} , bold black = 0, white = eastward, black = westward) during the 2010 SSW. **(a)** before the SSW (15 January), **(b)** during the SSW (30 January), **(c)** during the time of enhanced mixing (19 February) and **(d)** when the USLM vortex has reestablished (10 March). The black dashed vertical line marks the latitude of Sodankylä.

that the polar vortex did not recover to its original strength. The mid-latitude mesosphere especially at altitudes between 0.1 and 0.03 hPa is now drier than before the warming.

Vertical motion of air along WACCM TEM backward trajectories started at 67° N is shown in Fig. 5. The plot displays altitude changes per day against time and pressure 1, 2 and 3 days before the air reaches 67° N. The reason to display the data three days backward instead of just one is to show the similarity of the plots which indicates that the vertical displacement is nearly linear during the three days. Polar mid-winter 2010 is mostly dominated by subsidence of air (red colors) with the exception of the time during the SSW when upwelling in the mesosphere is evident from the blue colored area between 24 January and 7 February in Fig. 5. The upwelling appears to start in the upper mesosphere on approximately 27 January (approximately 0.03 hPa) and then propagates down towards the stratopause (in the lower mesosphere it starts at 30 January).

6 Water vapor in the polar middle atmosphere

MIAWARA-C's water vapor observations of winter 2010 support the above described scenario of horizontal mixing and vertical transport. The lower panel of Fig. 6 displays the time series of middle atmospheric water vapor over So-

dankylä as measured by MIAWARA-C. The upper panel shows the 67° N zonal mean water vapor obtained from MLS measurements. The plots indicate that, over Sodankylä and in zonal mean, mesospheric water vapor significantly increases by the end of January in the course of the SSW before it decreases throughout February. The temporal evolution of water vapor at different altitude levels as well as similarities and differences in the two time series, MIAWARA-C's point measurements and MLS's zonal mean, are described in Sect. 6.1. In Sect. 6.2 we show that the observed changes in mesospheric water vapor during and after the SSW 2010 can be attributed to transport processes. The humidification between 1 and 0.03 hPa at the onset of the SSW is partly due to horizontal advection from lower latitudes and partly due to vertical transport from lower mesospheric levels. The observed decrease in mesospheric water vapor after the SSW is shown to be caused by downward transport of air in the polar region.

6.1 Temporal evolution of water vapor

A direct comparison between the time-series of water vapor as observed by MIAWARA-C and MLS at stratopause height (1 hPa, approximately 46 km) and three mesospheric pressure levels (0.3, 0.1 and 0.03 hPa, approximately 54, 63 and 70 km), is given in Fig. 7. As expected the daily point

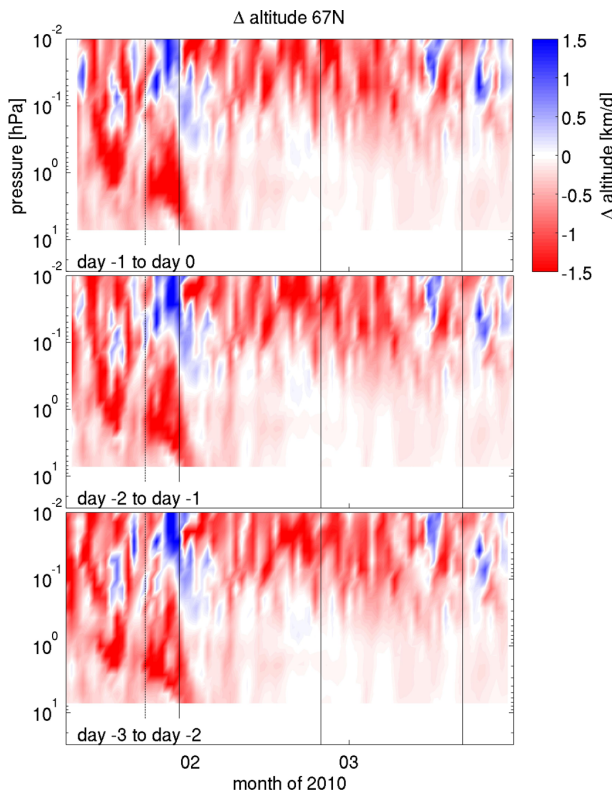


Fig. 5. Vertical motion along WACCM TEM backward trajectories started at 67° N. Daily altitude changes against time and pressure 1 day (top), 2 days (middle), and 3 days (bottom) backward, red indicates descent and blue ascent. The vertical lines indicate the following dates (from the left): 24 January (wind reversal mesosphere), 30 January (maximum temperature at 60° N and 10 hPa), 24 February (end of the time of enhanced meridional mixing) and 21 March (equinox).

measurements of MIAWARA-C (1- σ random uncertainty 5–18 % depending on altitude) show more variability than the zonal mean values of MLS (on average 56 profiles, 1- σ random uncertainty 1–5 % depending on altitude). This variability is due to a combination of measurement uncertainty and to small scale atmospheric fluctuations (e.g. non uniform H₂O distribution in combination with wind). Future investigations will be dedicated to the distinction between measurement uncertainty and atmospheric fluctuations as it is very difficult to separate the two sources of variability.

The effects of the 2010 SSW on mesospheric water vapor are most pronounced at pressures between 0.3 and 0.1 hPa. Before and during the warming the humidity at 0.1 hPa (0.3 hPa) rapidly increases from approximately 5 to 7 ppmv (5.5 to 7 ppmv) over Sodankylä and from approximately 5 to 6 ppmv (6 to 6.5 ppmv) in zonal mean. Whereas over Sodankylä the time of the increase coincides well with the time of the zonal wind reversal (24 January, first vertical line) the increase in zonal mean occurs a few days earlier. At 0.1 and 0.03 hPa the peak value in mesospheric water vapor oc-

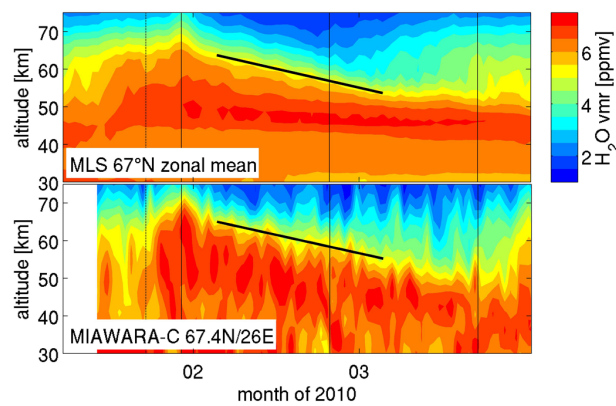


Fig. 6. Water vapor distribution in zonal mean at 67° N as measured by MLS (top) and over Sodankylä as measured by MIAWARA-C (bottom). Red indicates relatively higher values and blue relatively lower values. The black line marks the polar descent of dry mesospheric air. The descent rate is estimated as described in Sect. 7: linear fit to the 5.2 ppm isopleth of H₂O VMR for the time interval 5 February to 5 March. Descent rates are 350 m d⁻¹ for MIAWARA-C and 360 m d⁻¹ for MLS zonal mean. The vertical lines indicate the following dates (from the left): 24 January (wind reversal mesosphere), 30 January (maximum temperature at 60° N and 10 hPa), 24 February (end of the time of enhanced meridional mixing) and 21 March (equinox).

curs around 30 January in both times series. It is noteworthy that at the time of the maximum warming in the stratosphere (30 January, second vertical line) there is a rapid increase of nearly 1 ppmv at 0.1 and 0.03 hPa over Sodankylä and of approximately 0.5 ppmv at 0.03 hPa in zonal mean.

After 30 January water vapor gradually decreases at mesospheric altitudes while it stays approximately constant at stratopause level. At the highest level (0.03 hPa) the decrease from approximately 4 ppmv at the time of the maximum warming to less than 2 ppmv in mid-February is very rapid both over Sodankylä and in zonal mean. From the beginning of March the humidity starts to increase again. At 0.1 hPa the H₂O VMR decreases from more than 6 ppmv to less than 4 ppmv during February. In early March MIAWARA-C still observes a slight decrease over Sodankylä before H₂O starts to increase in mid-March while in zonal average the increase already starts in the beginning of March. At the lowest of the mesospheric levels (0.3 hPa) the H₂O VMR only decreases slightly throughout February. Here the dehydration starts in early March when humidity decreases from more than 6 ppmv to less than 5 ppmv. At the stratopause (1 hPa), water vapor stays more or less constant after the SSW with a slight decrease starting by mid-March. This is in agreement with the fact that at stratopause level H₂O is not well suited as a tracer for horizontal or vertical advection due to the maximum in VMR at these altitudes (Lee et al., 2011).

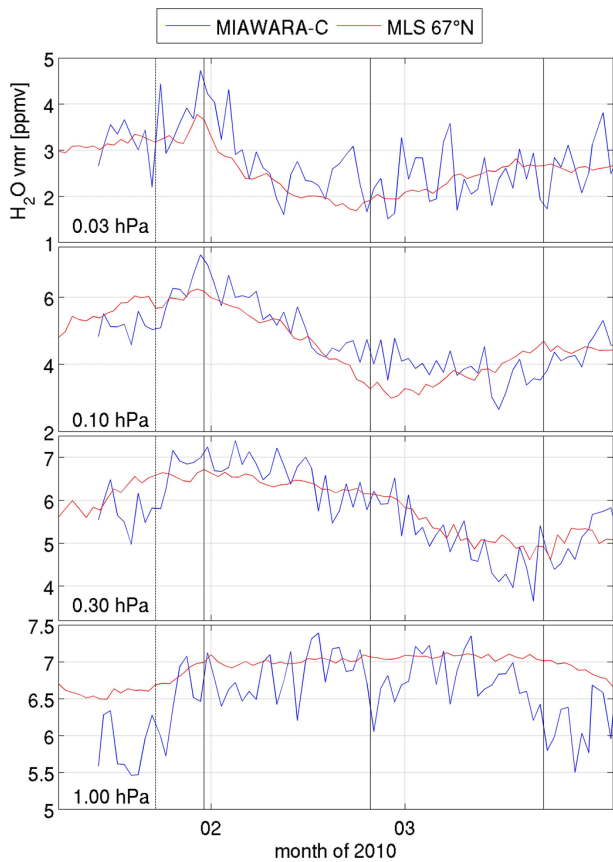


Fig. 7. Water vapor evolution on pressure levels at the stratopause (1 hPa) and in the mesosphere (0.3, 0.1 and 0.03 hPa) as observed by MIAWARA-C at 67.4° N, 26.6° E (blue) and MLS zonal mean at 67° N (red). The vertical lines indicate the following dates (from the left): 24 January (wind reversal mesosphere), 30 January (maximum temperature at 60° N and 10 hPa), 24 February (end of the time of enhanced meridional mixing) and 21 March (equinox).

6.2 Discussion of SSW-induced changes in dynamics and water vapor

In Fig. 8 water vapor values of MIAWARA-C are compared to MLS data along the backward trajectories 3 days prior to MIAWARA-C's measurement. The MLS data along the backward trajectories is found in the way described in Sect. 4.1. The two data sets are in good agreement indicating that the evolution of mesospheric water vapor can be mainly attributed to transport processes (horizontal and vertical). As mesospheric air within the vortex is drier than outside of it the good agreement in the water vapor data sets indicates that the Lagranto/ECMWF mesospheric trajectories allow to distinguish whether the air comes from inside or outside of the polar region.

The meridional origin (1, 2 and 3 days back, determined from Lagranto/ECMWF trajectories) of air masses sampled over Sodankylä against time and pressure is displayed in Fig. 9. Yellow and white colors indicate air transported from

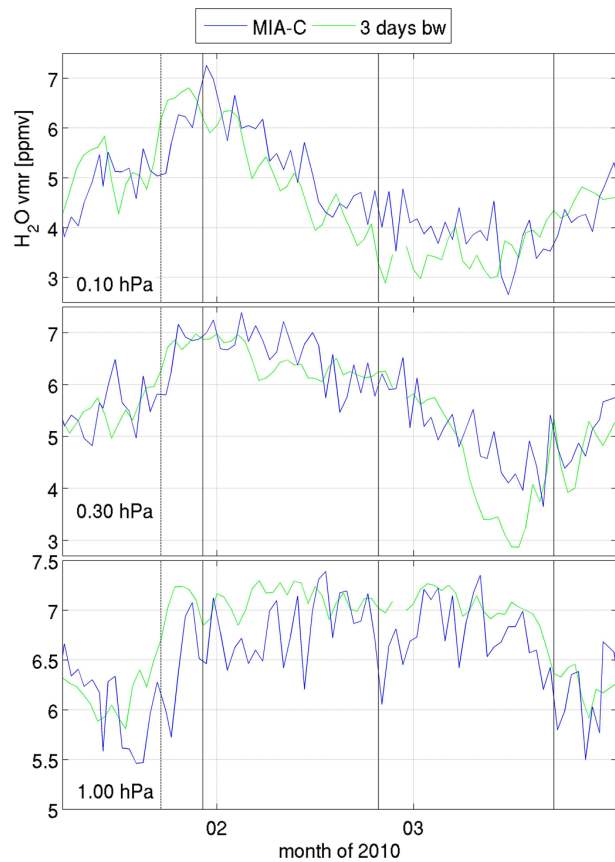


Fig. 8. Water vapor VMR along the trajectories on pressure levels at the stratopause (1 hPa) and in the mesosphere (0.3, 0.1 and 0.03 hPa). Curves are H₂O VMR on the day of MIAWARA-C's measurement (blue) and the value of MLS 3 days earlier at the location found by the trajectories (green). The vertical lines indicate the following dates (from the left): 24 January (wind reversal mesosphere), 30 January (maximum temperature at 60° N and 10 hPa), 24 February (end of the time of enhanced meridional mixing) and 21 March (equinox).

latitudes north of 60° N and orange and red colors south of it. The plots show that before the SSW stratospheric and lower mesospheric air over Sodankylä was already in the Arctic region 3 days prior to the measurement while the origin of upper mesospheric air parcels is mostly in mid-latitudes. This is consistent with the winter mean circulation transporting upper mesospheric air from low towards high latitudes where it descends into the polar vortex (compare e.g. Smith et al., 2011). During the SSW (around 26 January) the origin of middle atmospheric air over Sodankylä changes to subtropical regions which is a sign of strong meridional advection towards the Arctic. At the same time water vapor over Sodankylä starts to increase indicating meridional advection of air from mid-latitudes. Between 30 January and late February (third vertical line: 24 February) there was still air from lower latitudes being transported to Sodankylä. However, during this time the water vapor at the highest altitudes (0.1 and

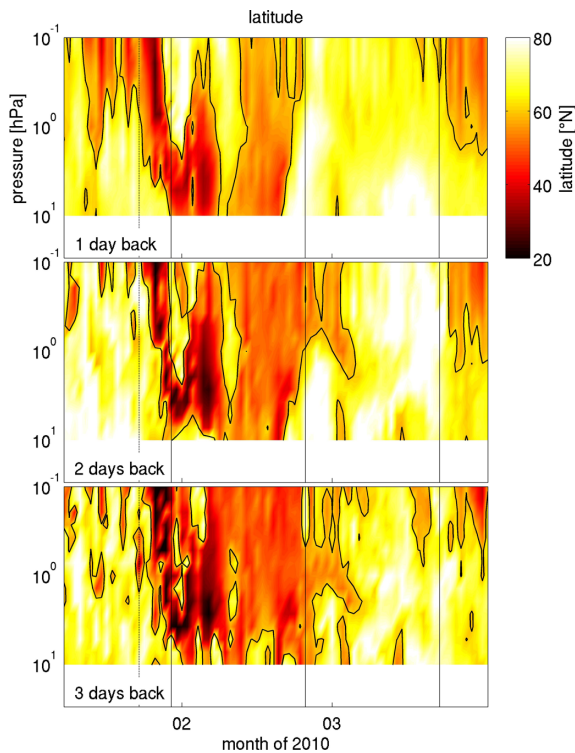


Fig. 9. Geographical origin (latitude) of measured air mass determined using Lagrangian trajectory calculations. Latitude of the air 1, 2 and 3 days before MIAWARA-C samples it over Sodankylä. White/yellow indicates polar latitudes and orange/red middle and subtropical latitudes. The black contour marks 60° N. The vertical lines indicate the following dates (from the left): 24 January (wind reversal mesosphere), 30 January (maximum temperature at 60° N and 10 hPa), 24 February (end of the time of enhanced meridional mixing) and 21 March (equinox).

0.03 hPa in Fig. 7) has already started to decrease indicating polar descent. From early to mid-March the air over Sodankylä is mostly of polar origin indicating that a (weak) mixing barrier has reformed and mesospheric water vapor is still decreasing at the lower altitudes (0.3 and 0.1 hPa) due to polar descent.

Polar projections of the 3-day backward trajectories started over Sodankylä at 1 hPa (left column) and 0.1 hPa (right column) are displayed in Fig. 10. Trajectories following an oval shape within the polar region indicate the existence of a regular eastward circulation (the polar vortex). Trajectories originating in low latitudes show low latitude air being transported towards Sodankylä indicating that the polar vortex has either been shifted away from northern Europe or broken down.

The plots pinpoint the circulation changes described above. In mid January at both altitudes the air reaching Sodankylä is following a regular circulation (polar vortex) which is disrupted by the SSW in the end of January. The disruption of the circulation is associated with advection of hu-

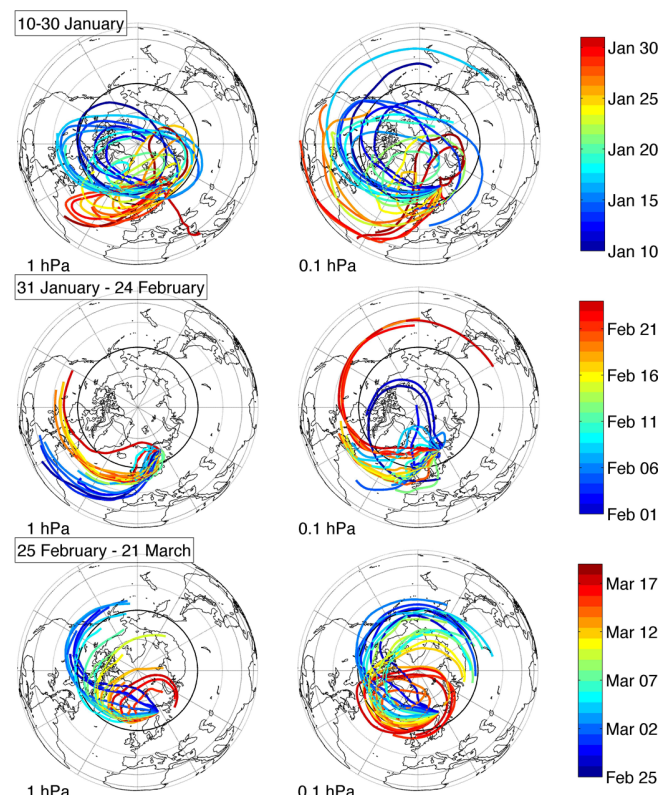


Fig. 10. 3-day LAGRANTO backward trajectories started over Sodankylä at 0.1 hPa (right) and 1 hPa (left). Starting dates are divided according to the three periods defined in Sect. 5.2. Top: time of the SSW (10–30 January), middle: time of enhanced meridional mixing (31 January–24 February), bottom: time of the USLM vortex (25 February–21 March). The colors of the trajectories indicate the starting date, blue being the earliest, red the latest. The black circle marks 60° N.

mid air from the subtropics to Sodankylä. The reason for the increase in lower mesospheric water vapor occurring earlier in zonal mean than over Sodankylä is that before the SSW the polar vortex with its dry mesospheric air was shifted towards Europe. Between the SSW and late February the circulation is still disturbed with trajectories originating at mid-latitudes following no distinct circulation pattern. This indicates large scale mixing of polar and mid-latitudinal air. In the period from early to mid-March a regular circulation has reestablished (USLM vortex).

Latitude-altitude cross section of TEM trajectories starting at altitudes of 3, 1, 0.3, 0.1 and 0.03 hPa and latitudes of 67° N are displayed in Fig. 11. They are used to gain further information about longer term (20 day) large scale horizontal advection and vertical transport. Panel a (15 January) indicates that before the SSW large scale air masses from high mesospheric altitudes in mid-latitude and even subtropical regions are transported into the Arctic mesosphere. The air at the stratopause and in the upper stratosphere is of polar mesospheric origin. At the time of the SSW (panel b, 30 January)

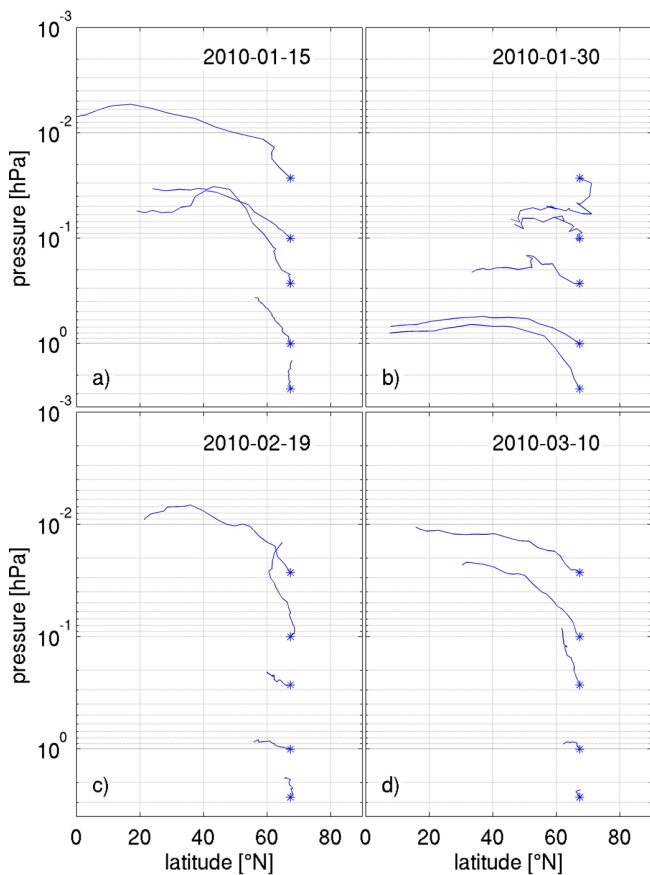


Fig. 11. Latitude-altitude cross section of 20-day backward TEM Trajectories started on 15 January, 30 January, 19 February and 10 March for the altitudes 3, 1, 0.3 , 0.1 and 0.03 hPa and the latitude 67° N. The end point of the backward trajectories is marked with a star.

the circulation changes. Now the meridional transport of mesospheric air is less pronounced while at the same time the air masses reaching the polar stratopause region have their 20-day back origin at the subtropical stratopause. This effect is associated with the strong stratospheric downwelling and simultaneous mesospheric upwelling in the polar region during the SSW. The short term water vapor increase at 0.03 and 0.1 hPa (Fig. 7), coinciding with the time of the maximum warming in the stratosphere on 30 January, is correlated with the mesospheric upwelling (Fig. 11b). Thus this water vapor increase is due to humid air transported upward from below.

By 19 February (panel c) the pre-warming circulation has started to reestablish above 0.01 hPa with air masses being transported from higher altitudes at mid-latitudes. At the lower levels the TEM trajectories indicate no transport towards Arctic regions. This is in contrast to the Lagrangian trajectories in Fig. 10 which have their 3-day back origin in mid-latitudes throughout February. This apparent contradiction is attributed to the presence of a planetary wave. Indications for such a wave can be seen in the Aura/MLS

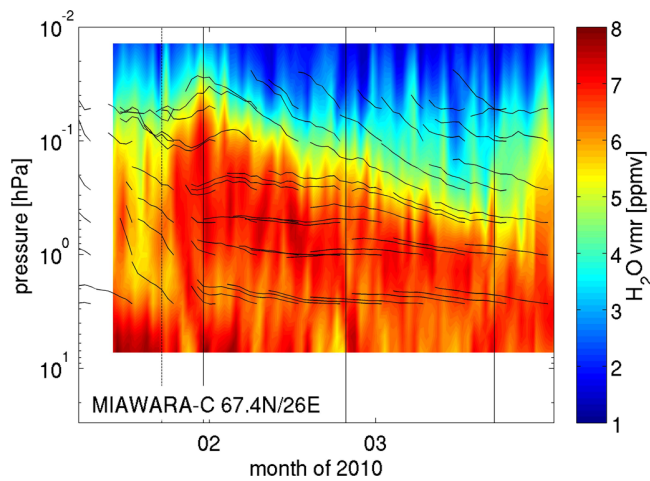


Fig. 12. H₂O measured by MIAWARA-C (colors, red relatively higher values, blue relatively lower values) and WACCM-TEM backward trajectories started every 7th day at 3, 1, 0.5, 0.3, 0.1, 0.05 hPa (black lines). The trajectories are only shown when the air mass sampled is in the polar region (north of 60° N). The vertical lines indicate the following dates (from the left): 24 January (wind reversal mesosphere), 30 January (maximum temperature at 60° N and 10 hPa), 24 February (end of the time of enhanced meridional mixing) and 21 March (equinox).

daily mesospheric maps (not shown). Horizontal trajectories follow the wave but there will be no net meridional transport (and therefore no TEM) unless the conditions for non-interaction are violated. In mid-March the USLM vortex has returned and a circulation similar to before the SSW, only weaker, is present.

A qualitative comparison between the downward advection as observed in MIAWARA-C's water vapor and the vertical coordinate of the 67° N TEM trajectories in the time they stay in the polar region is given in Fig. 12. The upwelling seen in the WACCM output before 30 January at altitudes above 0.1 hPa is in qualitative agreement with the increase in MIAWARA-C's water vapor at the same time and altitude. The polar descent at altitudes above 0.1 hPa throughout February observed by MIAWARA-C is confirmed by the vertical motion seen from the TEM trajectories.

There are two complementary explanations for the delayed water vapor decrease at 0.3 hPa: (1) the polar descent at this altitude is slow throughout February, evident from the TEM trajectories, (2) above 0.3 hPa water vapor is uniformly distributed after the humidification, evident from the water vapor distribution. Therefore at 0.3 hPa the slow polar descent cannot be seen in H₂O VMR before the beginning of March due to a lack of a vertical gradient.

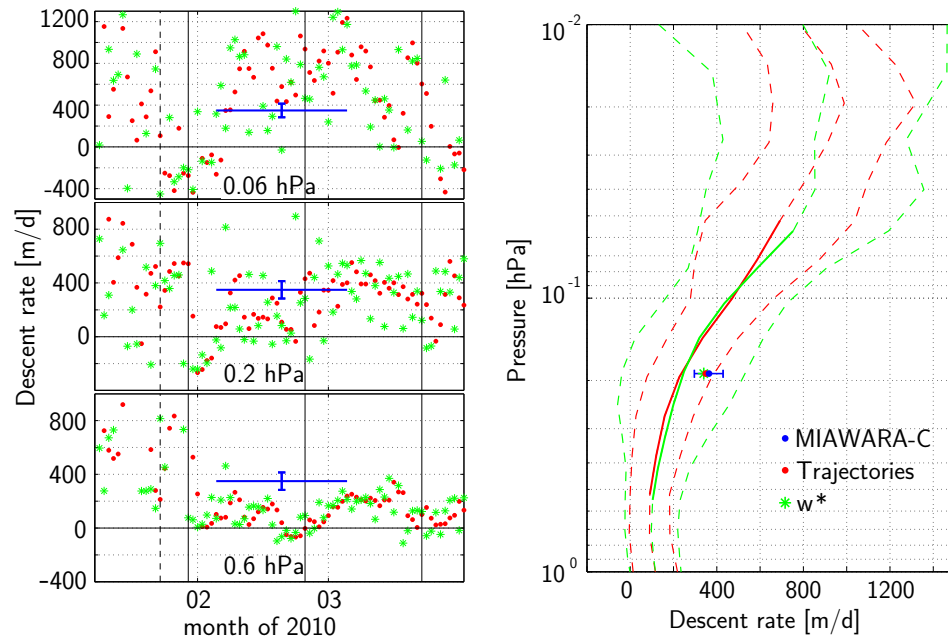


Fig. 13. Descent (or during the SSW ascent) rates at 67° N and over Sodankylä determined from TEM trajectories (red), w^* (green) and MIAWARA-C water vapor measurements (blue horizontal lines in the left panel and blue dot in the right panel). Left panel: daily vertical motion at the indicated altitude levels; positive values indicate descent, negative values ascent. The vertical lines indicate the following dates (from the left): 24 January (wind reversal mesosphere), 30 January (maximum temperature at 60° N and 10 hPa), 24 February (end of the time of enhanced meridional mixing) and 21 March (equinox). Right panel: mean value and standard deviation of daily descent rates between 5 February and 5 March. The solid part of the red and green curve indicates the altitude range covered by the 5.2 water vapor isopleth. The green asterisk, red and blue dots are the mean descent rates in that range found from TEM vertical wind and trajectories and determined from MIAWARA-C's measurements, respectively.

7 Determination of the polar descent rate

The descent rate of air after the 2010 SSW over Sodankylä and at 67° N is determined on one hand from TEM vertical motions and on the other hand from MIAWARA-C and MLS water vapor observations.

From the water vapor observations the descent rate is found by a least squares linear fit to the 5.2 ppmv water vapor isopleth. Assuming a relative uncertainty of 10 % (1.2 %) for MIAWARA-C's point measurements (MLS's zonal mean) we get an uncertainty of the isopleth altitude of 2.5 km (0.2 km). The determined descent rates and uncertainties are $350 \pm 40 \text{ m d}^{-1}$ for MIAWARA-C at Sodankylä and $360 \pm 5 \text{ m d}^{-1}$ for MLS zonal mean (valid for the interval 5 February to 5 March 2010 and the pressure range 0.6 to 0.06 hPa). The results of the polynomial fits together with the original data are displayed in Fig. 6. The values found are an average over altitude and time. Therefore the attribution of the descent rates to a certain altitude is imprecise.

The vertical motion from the TEM wind fields is given by either the vertical wind w^* or the vertical displacement along the trajectories. The information content of w^* and the along trajectory altitude change is slightly different; w^* indicates vertical displacement at a fixed latitude while the TEM trajectories follow the latitude change of the bulk motion of air

masses. The vertical motion along the backward trajectories is calculated by taking the difference between the along trajectory altitudes on day 0 and day -3 .

Assessment of errors in the atmospheric circulation of the WACCM model is subject to current research. Validation of the polar descent rate with direct measurements of the atmospheric wind field is difficult as winds between 40 and 80 km are poorly observed with only ground based radars providing profiles at altitudes between approximately 60 and 100 km. In addition, wind measurements from satellites are possible between approximately 80 and 100 km, e.g. TIDI/TIMED, but suffer under large uncertainties of between 7 and 15 m s^{-1} (Killeen et al., 2006). For that reason no errors are provided for the descent rates determined from WACCM data.

The descent rates from the TEM winds are displayed in Fig. 13 together with the value determined from MIAWARA-C's measurements. The left panel shows daily values at three different altitudes (0.6, 0.2 and 0.06 hPa) within the range covered by the 5.2 ppmv water vapor isopleth. The mean descent rate determined from water vapor, shown as blue horizontal line, is an altitude average and therefore shown on all three pressure levels.

The right panel shows the profiles of the temporal mean of descent rates with standard deviation, w^* in green and along

trajectory altitude change in red, for the time period in which the water vapor data has been considered for the linear fit (5 February to 5 March). The plot shows that the values of the two profiles are comparable. The descent rates from the TEM wind fields increase from approximately 80 m d^{-1} at 0.6 hPa to approximately 700 m d^{-1} at 0.06 hPa. The linear fit to the 5.2 ppmv H₂O isopleth provides a mean descent rate for the covered altitude range which is shown as blue dot in the right panel of Fig. 13. In order to make the descent rates determined from the TEM wind fields comparable to those from water vapor the mean value is taken over the same altitude range. This results in 335 m d^{-1} for the along trajectory altitude change (red dot) and in 325 m d^{-1} for w^* being in good agreement with the $350 \pm 40 \text{ m d}^{-1}$ found from MIAWARA-C's measurements.

The lower mesospheric descent rates determined are slightly smaller than the values of 500 to 700 m d^{-1} Lee et al. (2011) and Salmi et al. (2011) found after the 2009 SSW. In addition, the upper stratospheric descent rates in 2010 are slightly smaller than those of Nassar et al. (2005) who determined values of 150 m d^{-1} after the 2004 SSW. The smaller descent rates after the 2010 SSW compared to the two other years could indicate that the vortex recovery was weaker after the 2010 SSW than after the 2004 and 2009 SSW's.

8 Conclusions

This paper presents and interprets the evolution of mesospheric water vapor during the SSW of January 2010 as observed by the ground based radiometer MIAWARA-C stationed in the European Arctic. Lagrangian backward trajectory calculations show that the strong increase in mesospheric H₂O in the beginning of the SSW is associated with meridional advection of humid air from mid-latitudes. At the time of maximum temperature in the stratosphere there is a short term water vapor increase in the upper mesosphere (0.1 and 0.03 hPa) of nearly 1 ppmv over Sodankylä which is attributed to upwelling of humid air from lower altitudes. The upwelling is evident from the output of the SD-WACCM simulation and is indirectly confirmed by MIAWARA-C's water vapor observations.

After the SSW the northern middle atmosphere was disturbed for approximately 3 weeks. Lagrangian backward trajectories started above Sodankylä originated in middle latitudes and the MLS zonal mean distribution of water vapor indicated strong mixing. At the same time the SD-WACCM TEM trajectories showed no large scale advection of air masses from middle latitudes towards the Arctic. In March a weak vortex reestablished in the USLM region and the TEM circulation returned to a pattern similar to pre-SSW conditions. The rates of polar winter descent after the SSW determined from water vapor measurements are $350 \pm 40 \text{ m d}^{-1}$ over Sodankylä (MIAWARA-C) and $360 \pm 5 \text{ m d}^{-1}$ in zonal mean at 67° N (Aura/MLS). These values are consistent with

the 335 m d^{-1} altitude change along the TEM trajectories and the 325 m d^{-1} residual vertical wind from SD-WACCM. This shows that point measurements obtained from ground based microwave radiometers are well suited to detect and quantify dynamical large scale phenomena such as polar descent.

The combination of ground based and space borne microwave radiometers, Lagrangian trajectories from ECMWF operational data and SD-WACCM model data gave detailed results on transport processes in the polar winter atmosphere before, during and after the SSW of January 2010. There is a good agreement between polar descent as observed in MIAWARA-C's water vapor and the vertical component of the 67° N TEM trajectories (shown in Fig. 12). The similar mean descent rates indicate that the dynamics in the SD-WACCM model is consistent with the H₂O observations.

This study shows that the main features of transport during the SSW 2010 are reflected in the water vapor measurements by MLS as well as by MIAWARA-C. Ground based microwave radiometers can be used to study short term dynamical phenomena such as SSWs if their data is complemented with global fields from space borne instruments or models. Instrumental improvement of the ground based radiometers operated by the microwave group in Bern achieved in the past year has led to an increase in temporal resolution. The radiometers now deliver profiles approximately every 4 h which allows future studies of even shorter term phenomena such as atmospheric tides.

Acknowledgements. This work has been supported by the Swiss National Science Foundation grant number 200020-134684.

Participation at the Lapbiat campaign was funded through the EU Sixth Framework Program, Lapland Atmosphere-Biosphere Facility (LAPBIAT2). We thank the team of the Finnish Weather Service for their hospitality and support during the campaign.

In addition we thank Dominik Scheiben for providing a MATLAB interface to LAGRANTO and Mark Whale for correcting the English.

Particularly we like to thank the Bern University Research Foundation for funding the weather station of MIAWARA-C.

The National Center for Atmospheric Research is sponsored by the National Science Foundation.

Edited by: W. Ward

References

- Allen, D. R., Stanford, J. L., Nakamura, N., López-Valverde, M. A., López-Puertas, M., Taylor, F. W., and Remedios, J. J.: Antarctic polar descent and planetary wave activity observed in ISAMS CO from April to July 1992, *Geophys. Res. Lett.*, 27, 665–668, doi:10.1029/1999GL010888, 2000.
- Andrews, D. G. and McIntyre, M. E.: Planetary Waves in Horizontal and Vertical Shear: The Generalized Eliassen-Palm Relation and the Mean Zonal Acceleration, *J. Atmos. Sci.*, 33, 2031–2048,

- doi:10.1175/1520-0469(1976)033<2031:PWIHAV>2.0.CO;2, 1976.
- Andrews, D. G., Holton, J. R., and Leovy, C. B.: Middle atmosphere dynamics, Academic Press, Inc., London, 1987.
- Brasseur, G. P. and Solomon, S.: Aeronomy of the Middle Atmosphere, Springer, 3300 AA Dordrecht, Netherlands, third revised and enlarged edition, 2005.
- Brewer, A. W.: Evidence for a world circulation provided by the measurements of helium and water vapour distribution in the stratosphere, *Q. J. Roy. Meteorol. Soc.*, 75, 351–363, doi:10.1002/qj.49707532603, 1949.
- Charlton, A. J. and Polvani, L. M.: A New Look at Stratospheric Sudden Warmings. Part I: Climatology and Modeling Benchmarks, *J. Climate*, 20, 449–469, doi:10.1175/JCLI3996.1, 2006.
- Coy, L., Eckermann, S., and Hoppel, K.: Planetary Wave Breaking and Tropospheric Forcing as Seen in the Stratospheric Sudden Warming of 2006, *J. Atmos. Sci.*, 66, 495–507, doi:10.1175/2008JAS2784.1, 2009.
- de Wachter, E., Hocke, K., Flury, T., Scheiben, D., Kämpfer, N., Ka, S., and Oh, J. J.: Signatures of the Sudden Stratospheric Warming events of January–February 2008 in Seoul, S. Korea, *Adv. Space Res.*, 48, 1631–1637, doi:10.1016/j.asr.2011.08.002, 2011.
- ECMWF: IFS documentation for cycle 36r1, <http://www.ecmwf.int/research/ifsdocs/CY36r1/index.html>, 2012a.
- ECMWF: Evolution – Revisions during 2010, http://www.ecmwf.int/products/data/operational_system/evolution/evolution_2010.html, last access: 20 June 2012b.
- Flury, T., Hocke, K., Haefele, A., Kämpfer, N., and Lehmann, R.: Ozone depletion, water vapor increase, and PSC generation at midlatitudes by the 2008 major stratospheric warming, *J. Geophys. Res.*, 114, D18302, doi:10.1029/2009JD011940, 2009.
- Forkman, P., Eriksson, P., Murtagh, D., and Espy, P.: Observing the vertical branch of the mesospheric circulation at latitude 60°N using ground-based measurements of CO and H₂O, *J. Geophys. Res.*, 110, D05107, doi:10.1029/2004JD004916, 2005.
- Funke, B., López-Puertas, M., Bermejo-Pantaleón, D., García-Comas, M., Stiller, G. P., von Clarmann, T., Kiefer, M., and Linden, A.: Evidence for dynamical coupling from the lower atmosphere to the thermosphere during a major stratospheric warming, *Geophys. Res. Lett.*, 37, L13803, doi:10.1029/2010GL043619, 2010.
- Harada, Y., Goto, A., Hasegawa, H., Fujikawa, N., Naoe, H., and Hirooka, T.: A Major Stratospheric Sudden Warming Event in January 2009, *J. Atmos. Sci.*, 67, 2052–2069, doi:10.1175/2009JAS3320.1, 2010.
- Killeen, T. L., Wu, Q., Solomon, S. C., Ortland, D. A., Skinner, W. R., Niciejewski, R. J., and Gell, D. A.: TIMED Doppler Interferometer: Overview and recent results, *J. Geophys. Res.*, 111, A10S01, doi:10.1029/2005JA011484, 2006.
- Kinnison, D. E., Brasseur, G. P., Walters, S., Garcia, R. R., Marsh, D. R., Sassi, F., Harvey, V. L., Randall, C. E., Emmons, L., Lamarque, J. F., Hess, P., Orlando, J. J., Tie, X. X., Randel, W., Pan, L. L., Gettelman, A., Granier, C., Diehl, T., Niemeier, U., and Simmons, A. J.: Sensitivity of chemical tracers to meteorological parameters in the MOZART-3 chemical transport model, *J. Geophys. Res.*, 112, D20302, doi:10.1029/2006JD007879, 2007.
- Lamarque, J.-F., Emmons, L. K., Hess, P. G., Kinnison, D. E., Tilmes, S., Vitt, F., Heald, C. L., Holland, E. A., Lauritzen, P. H., Neu, J., Orlando, J. J., Rasch, P. J., and Tyndall, G. K.: CAM-chem: description and evaluation of interactive atmospheric chemistry in the Community Earth System Model, *Geosci. Model Dev.*, 5, 369–411, doi:10.5194/gmd-5-369-2012, 2012.
- Lambert, A., Read, W. G., Livesey, N. J., Santee, M. L., Manney, G. L., Froidevaux, L., Wu, D. L., Schwartz, M. J., Pumphrey, H. C., Jimenez, C., Nedoluha, G. E., Cofield, R. E., Cuddy, D. T., Daffer, W. H., Drouin, B. J., Fuller, R. A., Jarnot, R. F., Knosp, B. W., Pickett, H. M., Perun, V. S., Snyder, W. V., Stek, P. C., Thurstans, R. P., Wagner, P. A., Waters, J. W., Jucks, K. W., Toon, G. C., Stachnik, R. A., Bernath, P. F., Boone, C. D., Walker, K. A., Urban, J., Murtagh, D., Elkins, J. W., and Atlas, E.: Validation of the Aura Microwave Limb Sounder middle atmosphere water vapor and nitrous oxide measurements, *J. Geophys. Res.*, 112, D24S36, doi:10.1029/2007JD008724, 2007.
- Leblanc, T., Walsh, T. D., McDermid, I. S., Toon, G. C., Blavier, J.-F., Haines, B., Read, W. G., Herman, B., Fetzer, E., Sander, S., Pongetti, T., Whiteman, D. N., McGee, T. G., Twigg, L., Sunnicht, G., Venable, D., Calhoun, M., Dirisu, A., Hurst, D., Jordan, A., Hall, E., Miloshevich, L., Vömel, H., Straub, C., Kampfer, N., Nedoluha, G. E., Gomez, R. M., Holub, K., Gutman, S., Braun, J., Vanhove, T., Stiller, G., and Hauchecorne, A.: Measurements of Humidity in the Atmosphere and Validation Experiments (MOHAVE)-2009: overview of campaign operations and results, *Atmos. Meas. Tech.*, 4, 2579–2605, doi:10.5194/amt-4-2579-2011, 2011.
- Lee, J. N., Wu, D. L., Manney, G. L., Schwartz, M. J., Lambert, A., Livesey, N. J., Minschwaner, K. R., Pumphrey, H. C., and Read, W. G.: Aura Microwave Limb Sounder observations of the polar middle atmosphere: Dynamics and transport of CO and H₂O, *J. Geophys. Res.*, 116, D05110, doi:10.1029/2010JD014608, 2011.
- Liu, H. L. and Roble, R. G.: A study of a self-generated stratospheric sudden warming and its mesospheric-lower thermospheric impacts using the coupled TIME-GCM/CCM3, *J. Geophys. Res.*, 107, D23, doi:10.1029/2001JD001533, 2002.
- Liu, H.-L., Sassi, F., and Garcia, R. R.: Error Growth in a Whole Atmosphere Climate Model, *J. Atmos. Sci.*, 66, 173–186, doi:10.1175/2008JAS2825.1, 2008.
- Manney, G. L., Zurek, R. W., O'Neill, A., and Swinbank, R.: On The Motion Of Air Through The Stratospheric Polar Vortex, *J. Atmos. Sci.*, 51, 2973–2994, 1994.
- Manney, G. L., Krüger, K., Pawson, S., Minschwaner, K., Schwartz, M. J., Daffer, W. H., Livesey, N., Mlynaczak, M. G., Remsberg, E. E., Russell, J. M., and Waters, J. W.: The evolution of the stratopause during the 2006 major warming: Satellite data and assimilated meteorological analyses, *J. Geophys. Res.*, 113, D11115, doi:10.1029/2007JD009097, 2008.
- Manney, G. L., Harwood, R. S., MacKenzie, I. A., Minschwaner, K., Allen, D. R., Santee, M. L., Walker, K. A., Hegglin, M. I., Lambert, A., Pumphrey, H. C., Bernath, P. F., Boone, C. D., Schwartz, M. J., Livesey, N. J., Daffer, W. H., and Fuller, R. A.: Satellite observations and modeling of transport in the upper troposphere through the lower mesosphere during the 2006 major stratospheric sudden warming, *Atmos. Chem. Phys.*, 9, 4775–4795, doi:10.5194/acp-9-4775-2009, 2009a.
- Manney, G. L., Schwartz, M., Krueger, K., Santee, M., Pawson, S., Lee, J., Daffer, W., Fuller, R., and Livesey, N.: Aura Microwave Limb Sounder Observations of Dynamics and Transport During

- the Record-breaking 2009 Arctic Stratospheric Major Warming, *Geophys. Res. Lett.*, 36, L12815, doi:10.1029/2009GL038586, 2009b.
- Matsuno, T.: A Dynamical Model of the Stratospheric Sudden Warming., *J. Atmos. Sci.*, 28, 1479–1494, doi:10.1175/1520-0469(1971)028<1479:ADMOTS>2.0.CO;2, 1971.
- Monge-Sanz, B. M., Chipperfield, M. P., Simmons, A. J., and Uppala, S. M.: Mean age of air and transport in a CTM: Comparison of different ECMWF analyses, *Geophys. Res. Lett.*, 34, L04801, doi:10.1029/2006GL028515, 2007.
- Nassar, R., Bernath, P. F., Boone, C. D., Manney, G. L., McLeod, S. D., Rinsland, C. P., Skelton, R., and Walker, K. A.: ACE-FTS measurements across the edge of the winter 2004 Arctic vortex, *Geophys. Res. Lett.*, 32, L15S05, doi:10.1029/2005GL022671, 2005.
- Nezlin, Y., Rochon, Y. J., and Polavarapu, S.: Impact of tropospheric and stratospheric data assimilation on mesospheric prediction, *Tellus A*, 61, 154–159, doi:10.1111/j.1600-0870.2008.00368.x, 2009.
- Orsolini, Y. J., Urban, J., Murtagh, D., Lossow, S., and Limpasuvan, V.: Descent from the polar mesosphere and anomalously high stratopause observed in 8 years of water vapor and temperature satellite observations by the Odin Sub-Millimeter Radiometer, *J. Geophys. Res.*, 115, D12305, doi:10.1029/2009JD013501, 2010.
- Richter, J. H., Sassi, F., and Garcia, R. R.: Toward a Physically Based Gravity Wave Source Parameterization in a General Circulation Model, *J. Atmos. Sci.*, 67, 136–156, doi:10.1175/2009JAS3112.1, 2010.
- Salmi, S.-M., Verronen, P. T., Thölix, L., Kyrölä, E., Backman, L., Karpechko, A. Yu., and Seppälä, A.: Mesosphere-to-stratosphere descent of odd nitrogen in February–March 2009 after sudden stratospheric warming, *Atmos. Chem. Phys.*, 11, 4645–4655, doi:10.5194/acp-11-4645-2011, 2011.
- Seele, C. and Hartogh, P.: A case study on middle atmospheric water vapor transport during the February 1998 stratospheric warming, *Geophys. Res. Lett.*, 27, 3309–3312, doi:10.1029/2000GL011616, 2000.
- Siskind, D. E., Eckermann, S. D., Coy, L., McCormack, J. P., and Randall, C. E.: On recent interannual variability of the Arctic winter mesosphere: Implications for tracer descent, *Geophys. Res. Lett.*, 34, L09806, doi:10.1029/2007GL029293, 2007.
- Siskind, D. E., Eckermann, S. D., McCormack, J. P., Coy, L., Hoppel, K. W., and Baker, N. L.: Case studies of the mesospheric response to recent minor, major, and extended stratospheric warmings, *J. Geophys. Res.*, 115, D00N03, doi:10.1029/2010JD014114, 2010.
- Smith, A. K. K., Garcia, R. R., Marsh, D. R. R., and Richter, J. H.: WACCM Simulations of the Mean Circulation and Trace Species Transport in the Winter Mesosphere, *J. Geophys. Res.*, 116, D20115, doi:10.1029/2011JD016083, 2011.
- SPARC: Report on the Evaluation of Chemistry-Climate Models, in: Stratospheric Processes And their Role in Climate (SPARC), Report No. 5, edited by: Eyring, V., Shepherd, T. G., and Waugh, D. W., WCRP-132, WMO/TD-No. 1526, <http://www.atmosphys.physics.utoronto.ca/SPARC>, 2010.
- Stiller, G. P., Kiefer, M., Eckert, E., von Clarmann, T., Kellmann, S., García-Comas, M., Funke, B., Leblanc, T., Fetzer, E., Froidevaux, L., Gomez, M., Hall, E., Hurst, D., Jordan, A., Kämpfer, N., Lambert, A., McDermid, I. S., McGee, T., Miloshevich, L., Nedoluha, G., Read, W., Schneider, M., Schwartz, M., Straub, C., Toon, G., Twigg, L. W., Walker, K., and Whiteman, D. N.: Validation of MIPAS IMK/IAA temperature, water vapor, and ozone profiles with MOHAVE-2009 campaign measurements, *Atmos. Meas. Tech.*, 5, 289–320, doi:10.5194/amt-5-289-2012, 2012.
- Straub, C., Murk, A., and Kämpfer, N.: MIWARA-C, a new ground based water vapor radiometer for measurement campaigns, *Atmos. Meas. Tech.*, 3, 1271–1285, doi:10.5194/amt-3-1271-2010, 2010.
- Straub, C., Murk, A., Kämpfer, N., Golchert, S. H. W., Hochschild, G., Hallgren, K., and Hartogh, P.: ARIS-Campaign: intercomparison of three ground based 22 GHz radiometers for middle atmospheric water vapor at the Zugspitze in winter 2009, *Atmos. Meas. Tech.*, 4, 1979–1994, doi:10.5194/amt-4-1979-2011, 2011.
- Waters, J., Froidevaux, L., Harwood, R., Jarno, R., Pickett, H., Read, W., Siegel, P., Cofield, R., Filipiak, M., Flower, D., Holden, J., Lau, G., Livesey, N., Manney, G., Pumphrey, H., Santee, M., Wu, D., Cuddy, D., Lay, R., Loo, M., Perun, V., Schwartz, M., Stek, P., Thurstans, R., Boyles, M., Chandra, S., Chavez, M., Chen, G.-S., Chudasama, B., Dodge, R., Fuller, R., Girard, M., Jiang, J., Jiang, Y., Knosp, B., LaBelle, R., Lam, J., Lee, K., Miller, D., Oswald, J., Patel, N., Pukala, D., Quintero, O., Scaff, D., Snyder, W., Tope, M., Wagner, P., and Walch, M.: The Earth Observing System Microwave Limb Sounder (EOS MLS) on the Aura satellite, *IEEE T. Geosci. Remote Sens.*, 44, 1075–1092, 2006.
- Wernli, H. and Davies, H. C.: A lagrangian-based analysis of extratropical cyclones. I: The method and some applications, *Q. J. Roy. Meteorol. Soc.*, 123, 467–489, doi:10.1002/qj.49712353811, 1997.